Lateral Acceleration Control Design of a Non-Linear Homing Missile using Multi-Objective Evolutionary Optimisation

T. Sreenuch, A. Tsourdos, B. A. White and E. J. Hughes
Department of Aerospace, Power and Sensors, Cranfield University (RMCS)
Shrivenham, Swindon, SN6 8LA, UK
Email: T.Sreenuch, A.Tsourdos, B.A.White @rmcs.cranfield.ac.uk and ejhughes@iee.org

Abstract- The paper presents the lateral acceleration control design of non-linear missile model using a multi-objective evolutionary optimisation method (NSGA-II - like). The controller design for the uncertain plants is carried out by minimising gain and phase margins and tracking performance objectives of the corresponding vertices. Pareto surfaces are used to identify a feasible control structure and analyse its performance trade-offs. Based on the selected trade-off solution, the interpolated controller, whose poles, zeros and gains are linear continuous functions of Mach number and incidence, are designed for the whole operating envelope. The interpolated controller is now synthesised by minimising the Euclidean distance of multiple operating points' objective values. The stability is preserved by additionally overlapping these operating regions. The non-linear simulation results show that the resulting interpolated controller is indeed a robust tracking controller for all possible perturbations.

1 Introduction

This paper looks at the application of multi-objective evolutionary optimisation to a robust autopilot design. The aim is to synthesise the fixed-structure controller by shaping the open-loop frequency responses system's to lie outside the specified constant gain contour, as well results in the closed-loop responses are within the tracking bounds. However, finding a feasible control structure (and furthermore tuning it) that meet the frequency bounds can be very difficult, and the resulting interpolated controller may not be stabilising. By formulating the former to an optimisation problem, the Pareto optimal solutions of difference control structures can be searched using the Evolutionary Strategy and non-dominated ranking method. The feasible solutions can then be found and their trade-offs subsequently be analysed. Note that the ES also allows the inner and outer loop-shaping to be carried out simutaneously. To ensure the stability of the interpolated controller, the controllers' operating regions are required to be overlapped.

This paper is organised as follows. The missile's lateral dynamics and autopilot requirements are described in section 2. 2 DOF controller design using the frequency domain method and brief description of multi-objective evolutionary algorithms are stated in section 3. The gain-scheduling synthesis is presented in section 4.

2 Missile Model and Autopilot Requirements

2.1 Non-Linear Model

The missile model used in this study is taken from Horton's MSc thesis [Horton, 1992]. It describes a 5 DOF model in parametric format with severe cross-coupling and non-linear behaviour. This study will look at the reduced problem of a 2 DOF controller for the lateral motion (on the xy plane in Figure 1). The airframe is roll stabilised ($\lambda = 45°$),

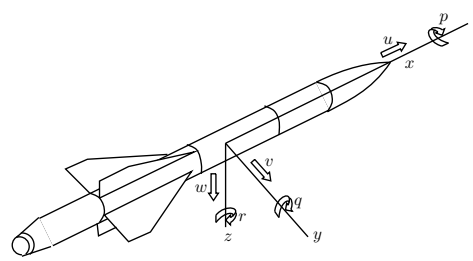

Figure 1: Airframe Axes and Nomenclature.

and no coupling is assumed between pitch and yaw channels. With these assumptions, the equations of motion are given by

$$\begin{aligned}
\dot{v} &= y_v(M,\sigma)v + y_\zeta(M,\sigma)\zeta - Ur, \\
&= \frac{1}{2m}\rho V S(C_{y_v}v + VC_{y_\zeta}\zeta) - Ur, \\
\dot{r} &= n_v(M,\sigma)v + n_r(M,\sigma)r + n_\zeta(M,\sigma)\zeta, \\
&= \frac{1}{2I_z}\rho V S d(C_{n_v}v + \frac{1}{2}dC_{n_r}r + VC_{n_\zeta}\zeta) \quad (1)
\end{aligned}$$

where the variables are defined in Figure 1. Here v is the side-slip velocity, r is the body rate, ζ the rudder fin deflections, y_v, y_ζ semi-non-dimensional force derivatives due to lateral velocity and fin angle, n_v, n_r, n_ζ semi-non-dimensional force derivatives due to side-slip velocity, body rate and fin angle. U is the forward velocity. Furthermore, $m = 150$ kg (125 kg) is the missile mass when full (all burnt), $\rho = \rho_0 - 0.094h$ air density ($\rho_0 = 1.23$ kg/m^3 is the sea level air density and h the missile altitude in km), V the total velocity in m/s, $S = \pi d^2/4 = 0.0314$ m^2 the reference area ($d = 0.2$ m is the reference diameter) and

$I_z = 75$ kg $\cdot$ m^2 (60 kg $\cdot$ m^2) is the lateral inertia when full (all burnt). For the coefficients C_{y_v}, C_{y_ζ}, C_{n_v}, C_{n_r}, C_{n_ζ} only discrete data points are available, obtained from wind tunnel experiments. The interpolation formulas, involving the Mach number M and incidence σ, have been evaluated with the results summarised in Table 1.

Aerodynamic derivative	Interpolated formula
C_{y_v}	$-26 + 1.5M - 60\|\sigma\|$
C_{y_ζ}	$-10 + 1.4M - 1.5\|\sigma\|$
C_{n_r}	$-500 - 30M + 200\|\sigma\|$
C_{n_v}	$s_m C_{y_v}$, where $s_m = d^{-1}[(1.3 + m/500) - (1.3 + 0.1M + 0.3\|\sigma\|)]$
C_{n_ζ}	$s_f C_{y_\zeta}$, where $s_f = d^{-1}[(1.3 + m/500) - 2.6]$

Table 1: Aerodynamic Derivatives of the Non-Linear Model ($\lambda = 45°$).

$V = \sqrt{U^2 + v^2}$ is to total velocity. It is assumed that $U \gg v$, so that the total incidence σ can thus be taken as $\sigma = v/U$, as $\sin\sigma \approx \sigma$ for small σ. Finally, the Mach number is obviously defined as $M = V/a$, where $a = 340$ m/s is the speed of sound.

2.2 Closed-Loop Performance Requirements

The autopilot is required to track ± 500 m/s^2 lateral acceleration commands a_{y_d} over the whole flight envelope (see Figure 2). Note that the lateral acceleration

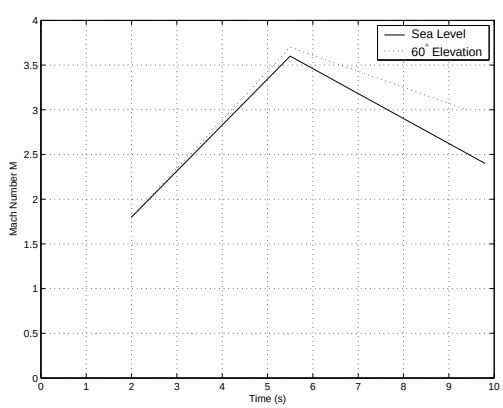

Figure 2: Velocity Operating Envelope.

a_y at the center of gravity is defined by $a_y = \dot{v} + Ur$. It must also be as robust to the variation in mass (see Figure 3) and uncertainty in aerodynamic derivatives ($\Delta_{C_{y_v}}, \Delta_{C_{y_\zeta}}, \Delta_{C_{n_v}}, \Delta_{C_{n_r}}, \Delta_{C_{n_\zeta}} = \pm 5\%$). A list of performance specification (for a step input) is given in the time-domain using familiar figures as follows:

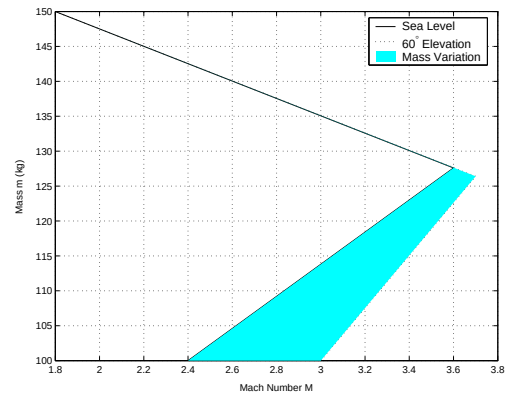

Figure 3: Mass Variations. The Propellant is Constantly Burnt.

1. Steady state gain $0.9 \leq \left.\frac{a_y(s)}{a_{y_d}(s)}\right|_{s=0} \leq 1.1$,
2. Settling time $0.1 \leq t_s \leq 0.3$,
3. Damping ratio $0.6 \leq \zeta_{a_y} \leq 0.8$,
4. Gain margin $GM \geq 9$ dB, Phase margin $PM \geq 40°$.

3 Design of Lateral Missile Autopilot

3.1 2 DOF Autopilot Configuration

The basic 2 DOF lateral autopilot is shown schematically in Figure 4 where $l_a = 0.9$ m (0.8 m) is the accelerometer moment arm when full (all burnt). By linearising the nonlinear

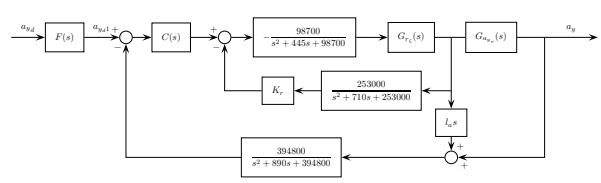

Figure 4: 2 DOF Autopilot Configuration.

dynamic equation (1) about an operating point results in the transfer functions:

$$G_{r_\zeta}(s) = \frac{n_\zeta s - (n_\zeta y_v - n_v y_\zeta)}{s^2 - (y_v + n_r)s + (U n_v + y_v n_r)},$$
$$G_{a_{y_r}}(s) = \frac{y_\zeta s^2 - y_\zeta n_r s - U(n_\zeta y_v - n_v y_\zeta)}{n_\zeta s - (n_\zeta y_v - n_v y_\zeta)}. \quad (2)$$

3.2 Frequency-Response Design Method

3.2.1 Tracking Models

In this work, the desired tracking ratios are modeled in the frequency domain to satisfy the required gain and phase margins and the desired time domain performance specifications (see section 2.2). The system's tracking performance specifications are based upon satisfying all of the step forcing functions $T_U(t)$ and $T_L(t)$ shown in Figure 5, where $T_U(s) = (34.43s + 4889)(s^2 + 80s + 4444)$ and $T_L(s) = 2.503 \times 10^4/(s^3 + 84.5s^2 + 2405s + 2.781 \times 10^4)$. They represent the upper and lower bounds of tracking performance specifications whom an acceptable response $a_y(t)$ must lie within. The Bode plot of the upper bound $T_U(j\omega)$ and lower bound $T_L(j\omega)$ for $|T(j\omega)| = |a_y(j\omega)/a_{yd}(j\omega)|$ are shown in Figure 6.

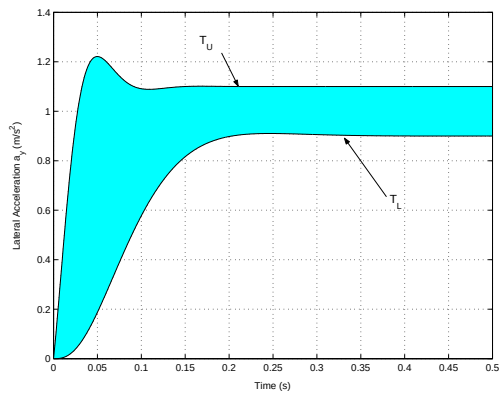

Figure 5: Time Domain Response Specifications.

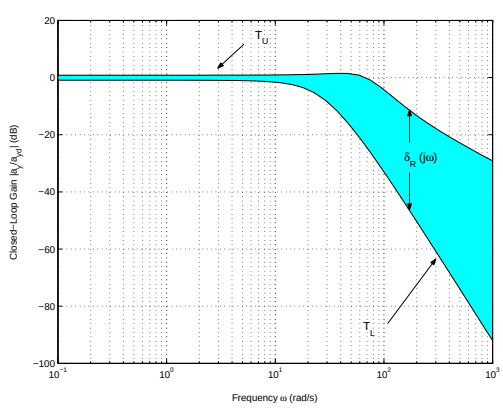

Figure 6: Frequency Domain Response specifications.

3.2.2 Loop-shaping

A robust controller can be designed by synthesising a rate feedback K_r and compensator $C(s)$ that 1) results in an open-loop transmission $L(j\omega)$ satisfies the desired gain and phase margins. 2) results in the closed-loop magnitude variation $\delta_T(j\omega_i)$ being smaller than or equal to $\delta(j\omega_i)$ of Figure 6, i.e. high open-loop gain $|L(j\omega)|$ is usually a consequence (see Figure 8). 3) results in $T_L(j\omega_i) \leq T(j\omega_i) \leq T_U(j\omega_i)$ (If it is not possible, further design of a prefilter $F(s)$ is required.) [Houpis and Rasmussen, 1999].

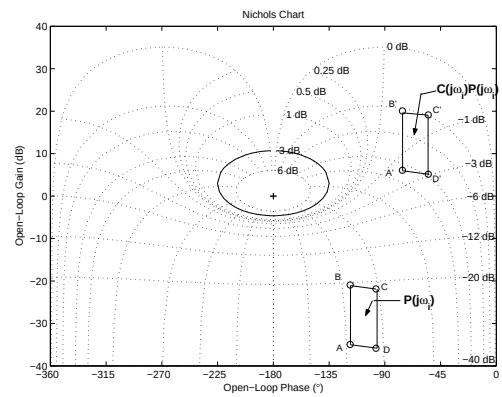

Figure 7: Nichols Chart (In unity-feedback case, $\delta_T(j\omega_i)$ is attenuated as a result of high open-loop gain $|L(j\omega_i)|$).

With these design objectives, the resulting controller's performance can then be measured by evaluating the following robustness assessment functions:

Gain and Phase Margins Based Cost Function

A look at the Nichols Chart qualitatively reveals that gain and phase margin can be defined in term of $\max_{\omega} |T(j\omega)|$. For instance, if $|T(j\omega)| \leq 3$ dB, it is guaranteed that $GM > 4$ dB and $PM > 45°$ (see Figure 7) [Sidi, 2001].

Adopting these relationships, the gain and phase margin based cost function can be given by

$$J_{1_i} = \max_{\omega_L \leq \omega \leq \omega_U} \frac{|T_{1_i}(j\omega)| + \gamma_0}{\gamma + \gamma_0}, \tag{3}$$

where $i = 1, \ldots, NOV$ is the vertices index, $T_1(j\omega) = a_y(j\omega)/a_{y_{d1}}(j\omega)$ and γ_0 is some unity-feedback constant gain contour.

By using a standard block diagram reduction rules, $L(s)$ can be written as

$$L(s) = \frac{-C(s)J(s)(l_a s G_{r_\zeta}(s) + G_{a_{y_\zeta}}(s))H_{a_y}(s)}{1 - K_r F(s) G_{r_\zeta}(s) H_r(s)}, \tag{4}$$

where $J(s)$, $H_r(s)$, $H_{a_y}(s)$ are fin servo, rate gyro and accelerometer dynamics, respectively. Note that $|l_a(j\omega)G_{r_\zeta}(j\omega) + G_{a_{y_\zeta}}(j\omega)| \leq |G_{a_{y_\zeta}}(j\omega)|$ and $\angle l_a(j\omega)G_{r_\zeta}(j\omega) + G_{a_{y_\zeta}}(j\omega) \geq \angle G_{a_{y_\zeta}}(j\omega)$ (see Figure

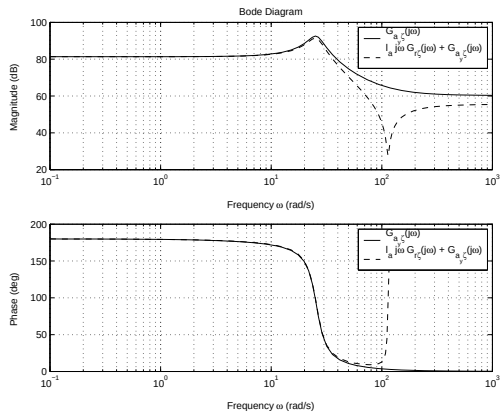

Figure 8: Frequency Responses of $G_{a_{y_\zeta}}(j\omega)$ and $l_a(j\omega)G_{r_\zeta} + G_{a_{y_\zeta}}$ (linearised at $M = 3.0$ and $\sigma = 2.5°$).

8). Thus, if the relative stability condition is satisfied ($J_{1_i} \leq 1$), then the achieved margins will be greater than or equal to the designed values.

Tracking Boundaries Based Cost Function
Consider the tracking specifications given in Figure 6, the upper tracking boundary cost function can be defined by,

$$J_{U_i} = \max_{\omega_L \leq \omega \leq \omega_U} \frac{|T_i(j\omega)| - |T_R(j\omega)|}{|T_U(j\omega)| - |T_R(j\omega)|}, \tag{5}$$

where $T_R(j\omega)$ is a nominal tracking frequency responses. Similarly for the lower tracking bound case

$$J_{L_i} = \max_{\omega_L \leq \omega \leq \omega_U} \frac{|T_R(j\omega)| - |T_i(j\omega)|}{|T_R(j\omega)| - |T_L(j\omega)|}. \tag{6}$$

Taking both J_{U_i} and J_{L_i} into account, a composite cost function can therefore be written as

$$J_{2_i} = \max\{J_{U_i}, J_{L_i}\} \tag{7}$$

(shaded region in Figure 6).

3.3 Controller Parameters Tuning via Multi-Objective Optimisation

3.3.1 Multi-Objective Optimisation using Evolution Strategies

Basic scheme of the $(\mu + \lambda)$-ES's used in this paper is as that described in [Deb, 2001, Hughes et al., 2003]. Each ES trial starts with random variable vectors $\vec{x}$ of μ individuals whose initial strategy parameters are chosen as $\vec{\sigma} = (\vec{x}_U - \vec{x}_L)/8$ where $\vec{x}_U, \vec{x}_L$ are variable vectors' upper and lower bounds, respectively. At each generation, λ offsprings are created through recombination and mutation described below:

Intermediate Crossover
For any randomly chosen parents $(\vec{x}^1, \vec{\sigma}^1)$ and $(\vec{x}^2, \vec{\sigma}^2)$, an offspring $(\vec{x}, \vec{\sigma})$ is computed from

$$\begin{aligned} x_i &= \gamma_i x_i^1 + (1 - \gamma_i) x_i^2, \\ \sigma_i &= \beta_i \sigma_i^1 + (1 - \beta_i) \sigma_i^2, \end{aligned} \tag{8}$$

where γ_i and β_i are random numbers between -0.25 and 1.25.

Non-Isotropic Self-Adaption
Given an offspring $(\vec{x}, \vec{\sigma})$, a resulting mutated offspring $(\vec{x}', \vec{\sigma}')$ is calculated by using the logarithmic update rules

$$\begin{aligned} \sigma_i' &= \sigma_i \exp(\tau' N(0,1) + \tau N_i(0,1)), \\ x_i' &= x_i + \sigma_i' N_i(0,1), \end{aligned} \tag{9}$$

where $N(0,1)$ and $N_i(0,1)$ are one-dimensional normally distributed random variables with zero mean and unity standard deviation. The parameter τ' and τ are learning parameters which are set as $\tau' = (2n)^{-1/2}$ and $\tau = (2n^{1/2})^{-1/2}$, where n is the dimension of the variable vector.

After that, a selection pool of $\mu + \lambda$ solutions is formed. The objective values are evaluated (J_{1_i}, J_{2_i} in section 3.2.2) and then sorted (see below). The best μ solutions will be chosen as new parents using non-dominated ranking described as follows:

Elitist Non-Dominated Selection
A selection procedure used here is as NSGA-II described in [Deb, 2001]. Each generation, $\mu + \lambda$ solutions are first classified using a non-dominated sorting. The best μ solutions are selected from the solutions of different non-dominating fronts F_j, one at a time. However, when the last allowed front F_M is being considered, there may exist more solutions than the remaining required solutions (i.e. $\sum_{j=1}^{M} |F_j| > \mu$). In stead of arbitrarily discarding some members from F_M, the most widely spread $\mu - \sum_{j=1}^{M-1} |F_j|$ solutions are included using the crowding distance values defined as

Crowding Distance Assignment Procedure:

3 For each $n = 1, \ldots, |F_M|$, set $d_n = 0$.

2 For each objective function $m = 1, \ldots,$ NOBJ, find the sorted indices vector $I^m = \text{sort}(f_m, >)$.

3 For $m = 1, \ldots,$ NOBJ, assign $d_{I_1^m} = d_{I_{|F_M|}^m} = \infty$,

and for all other solutions $n = 2, \ldots, |F_M| - 1$, assign:

$$d_{I_n^m} = d_{I_n^m} + \frac{f_m^{I_{n+1}^m} - f_m^{I_{n-1}^m}}{f_m^{max} - f_m^{min}} \tag{10}$$

where I_n denotes the solution index of the nth member in the sorted list I^m. $f_m^{max} = \max_{x \in F_M} f_m(x)$, and similarly for f_m^{min}.

3.3.2 Implication of Trade-Offs

Suppose the controller's order is prespecified (e.g. K_r, $C(s) = K_p(s+z_p)/(s+p_p)$, and $F(s) = K_f(s+z_f)/(s+p_f)$). Then, the optimisation variables are K_r, K_p, z_p, p_p, K_f, z_f and p_f. This is similar for difference control structures.

To ensure internal stability, it is desired that a minimum phase and stable controller is designed. Since there is no prior information about the range of the parameters in the controller, the quite large ranges of all parameters (e.g. $[10^{-7}, 10^4]$) are chosen. Likewise classical loop-shaping, these set of parameters are then translated into the logarithmic space (i.e. $[10^{-7}, 10^4]$ now becomes $[-7, 4]$), thus

$$\vec{x} = [\bar{K}_r, \bar{K}_p, \bar{z}_p, \bar{p}_p, \bar{K}_f, \bar{z}_f, \bar{p}_f], \tag{11}$$

where $\bar{K}_r = \log_{10} K_r$, $\bar{K}_p = \log_{10} K_p$, etc..., is now formed a variables vector for the ES. This also proves to speed up the convergence of the ES [Chen et al., 1998].

Consider the operating region $2.5 \leq M \leq 3.5$ and $0.0 \leq \sigma \leq 5.0$. Let $\gamma_0 = -6$ dB, $\gamma = 3$ dB, $T_R(s) = 1451/(s^2 + 53.33s + 1451)$, $T_U(s) = (34.43s + 4889)/(s^2 + 80s + 4444)$ and $T_L(s) = 2.503 \times 10^4/(s^3 + 84.5s^2 + 2405s + 2.781 \times 10^4)$. Pursuing the method described in section 3.3.1 (using (100+100)-ES), the Pareto-optimal solutions for difference control structures are shown in Figure 9.

It can be seen that the requirements given in section 2.2 is satisfied with 1st-order $C(s)$ and 1st-order $F(s)$. Its three difference Pareto-optimal solutions are shown in Figure 10. The solution with minimum tracking performance index while satisfying gain and phase margin requirements ($J_1 < 1$) is usually preferred (i.e. solution A in Figure 10). However, the phase margin are significantly decreased relatively compared to a slight improvement in tracking performance (see Figure 11 and 12). In addition, when the designed controllers are interpolated, the performance degradations of the resulting controller is likely in this case. But then gain and phase margins are the constraints that must be met, hence such compromised solution as B is preferred in this case. The step responses of the vertex systems are shown in Figure 13.

Note that the influence of a non-minimum phase zero z_{NMP} on the output response is expected (i.e.an undershoot

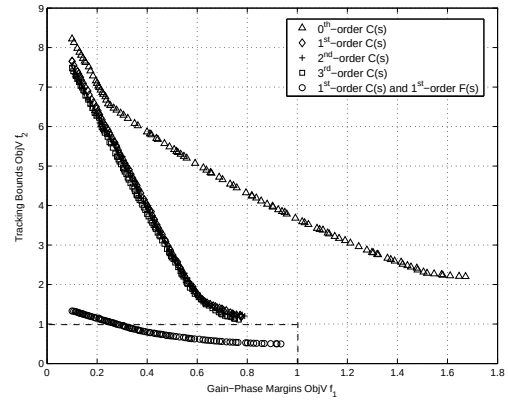

Figure 9: Pareto-Optimal Solutions for Difference Control Structures (at 500th-generation).

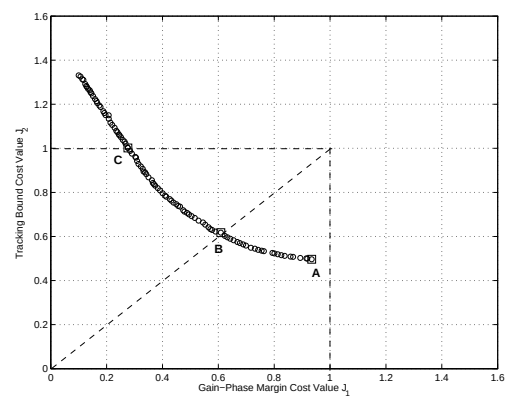

Figure 10: Three Pareto-Optimal Solutions for 1st-order $C(s)$ and $F(s)$ configuration.

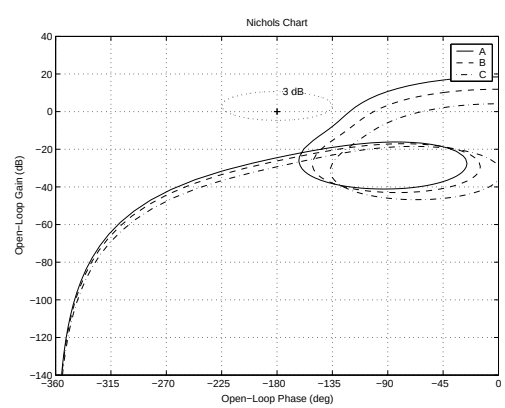

Figure 11: Nominal Open-Loop Responses of Difference Paretor-Optimal Solutions.

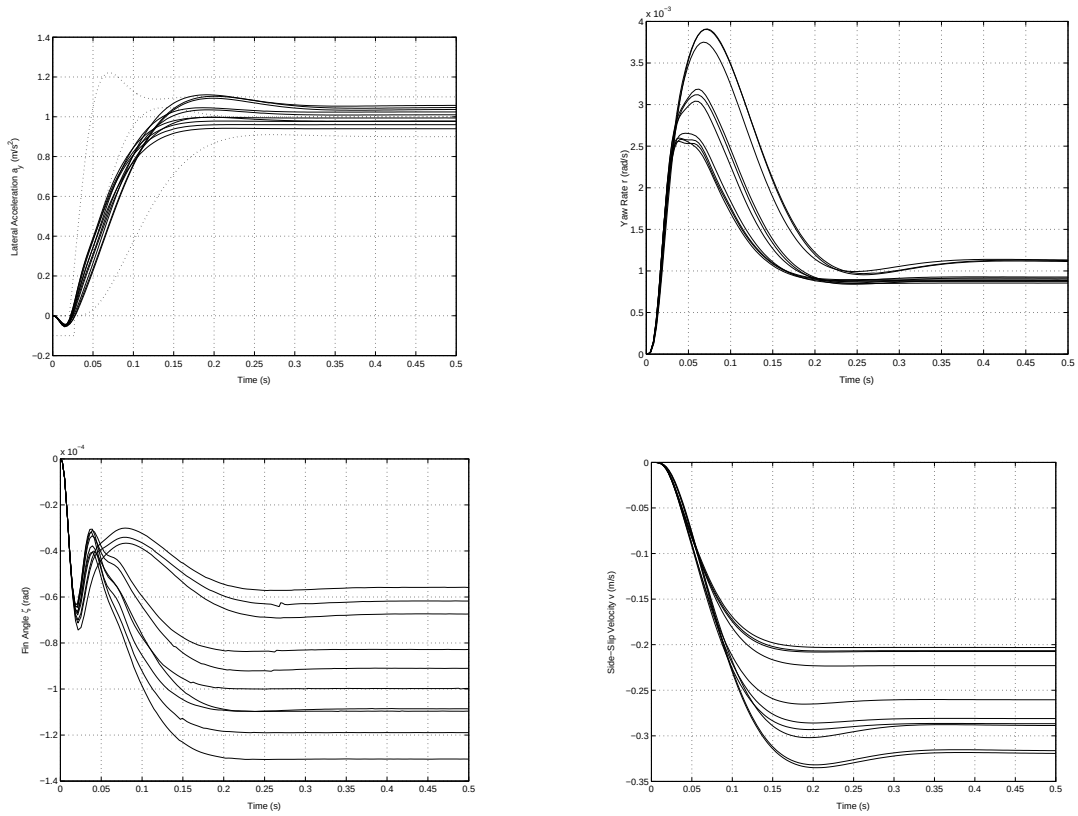

Figure 13: Step Responses of the Vertex Systems.

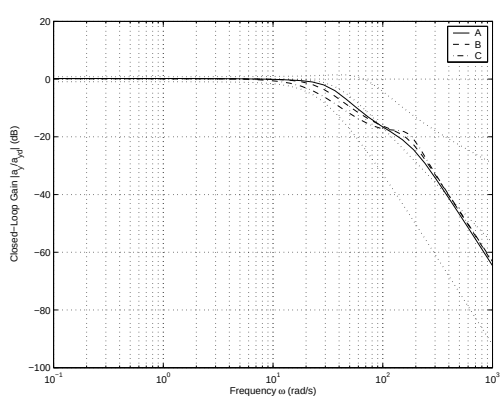

Figure 12: Nominal Closed-Loop Responses of Difference Pareto-Optimal Solutions.

and delay in the output response). Using 1st-order Padé approximation, a time delay T_d is calculated to be $2/z_{NMP}$ [Franklin et al., 1994].

4 Robust Gain-Scheduled Controller

4.1 Stability Preserving Interpolation Method

To obtain the non-linear controller, following the previous design method, K_r, $C(s)$ and $F(s)$ must be designed for each operating point. By using a fixed control structure ($C(s) = K_p(s+z_p)/(s+p_p)$, $F(s) = K_f(s+z_f)/(s+p_f)$ in this case), the controllers are then interpolated by linear interpolation of poles, zeros and gains. However, to ensure the stability of the interpolated controller, these operating regions must be overlap [Stilwell and Rugh, 2000] (see Figure 14).

4.2 Design of Linear Interpolated Controller

Instead of using piecewise linear interpolation, the controller's poles, zeros and gains are prespecified as linear functions of Mach number M and incidence σ (e.g. $K_r = k_{r_0} + k_{r_M} M + k_{r_\sigma}|\sigma|$), whose coefficients straightforwardly are the optimisation variables (k_{r_0}, k_{r_M},...,$k_{p_{f_\sigma}}$). Following the trade-offs implication in section 3.3.2, the compos-

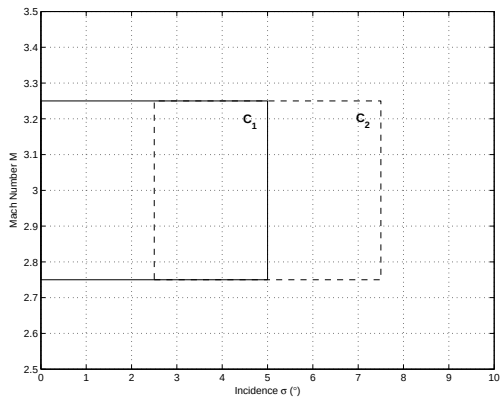

Figure 14: Two Scheduled Controllers.

ite objective values at each design point $n = 1, \ldots, NOC$ is given by

$$J^n = \max_{i=1,\ldots,NOV} \{J^n_{1_i}, J^n_{2_i}\}. \tag{12}$$

These objective values $J^n = 1, \ldots, NOC$ are then combined into a single objective value J using a Euclidean distance given by

$$J = \left(\sum_{n=1}^{NOC} |J^n|^2 \right)^{1/2}. \tag{13}$$

This is sufficient since the previously obtained Pareto-optimal solutions are convex.

The design is now carried out by minimising (13) (using (1,000+1,000)-ES) which results are in Figure 15 and 16 and Table 2. The resulting controller well satisfies the performance specifications in all operating regions (i.e. $J^n < 1$ in Figure 16). Note that $\vec{x} = [\bar{k}_{r_0}, \bar{k}_{r_M}, \ldots, \bar{k}_{p_{f_\sigma}}]$ is as previously formed a variables vector for the ES. Employing the non-linear 2 DOF model described in section 2.1, the time responses of the interpolated controller are shown in Figure 17.

Poles, Zeros and Gains	Interpolated formula
K_r	$0.04975 - 3.7895 \times 10^{-6}M + 4.0004 \times 10^{-5}\lvert\sigma\rvert$
K_p	$0.00019776 - 2.5921 \times 10^{-6}M - 7.4025 \times 10^{-6}\lvert\sigma\rvert$
z_p	$29.7157 + 2.0687M + 0.14944\lvert\sigma\rvert$
p_p	$11.7764 - 0.0071308M + 0.83534\lvert\sigma\rvert$
K_f	$0.007496 + 0.0003413M + 0.00028804\lvert\sigma\rvert$
z_f	$3569.8013 - 6.9168M - 7.5136\lvert\sigma\rvert$
p_f	$21.5537 + 1.0348M - 8.1409\lvert\sigma\rvert$

Table 2: Poles, Zeros and Gains Interpolated Formulas.

5 Conclusions

The paper presents the lateral acceleration control design of a non-linear missile model using the multi-objective evolutionary optimisation method. The design is carried out by shaping the uncertain open-loop responses to lie outside the specified constant gain contour, as well results in the uncertain closed-loop responses are within the tracking bounds (in this case an additional 1st-prefilter is required). Using the Pareto surfaces, the feasible control structure is identified and its performance trade-offs are analysed. The unity weighted Min-Max solution is chosen as a decision choice.

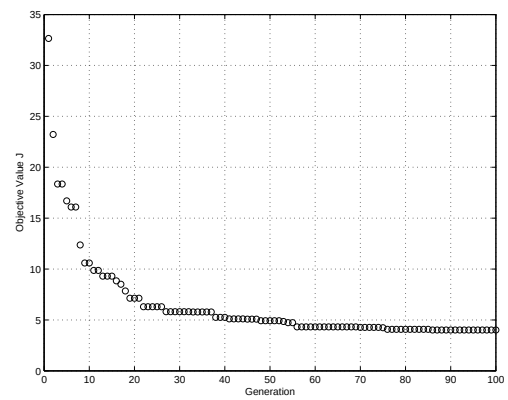

Figure 15: The Convergence History of the Solution Representing the Best Controller.

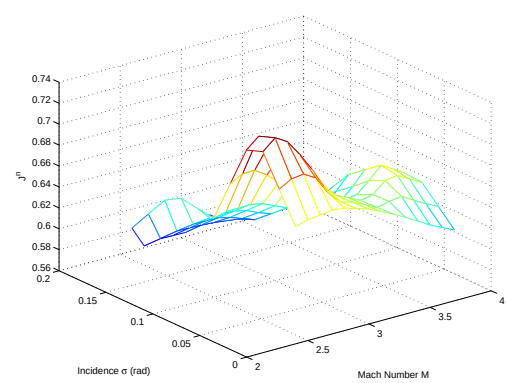

Figure 16: The Objective Values J^n.

To obtain the non-linear controller, the interpolated controller, whose poles, zeros and gains are linear continuous functions of Mach number M and incidence σ, are designed for the whole operating envelope. The controller is synthesised by minimising the Euclidean distance of multiple operating points' objective values. The non-linear simulation results show that the resulting interpolated controller is

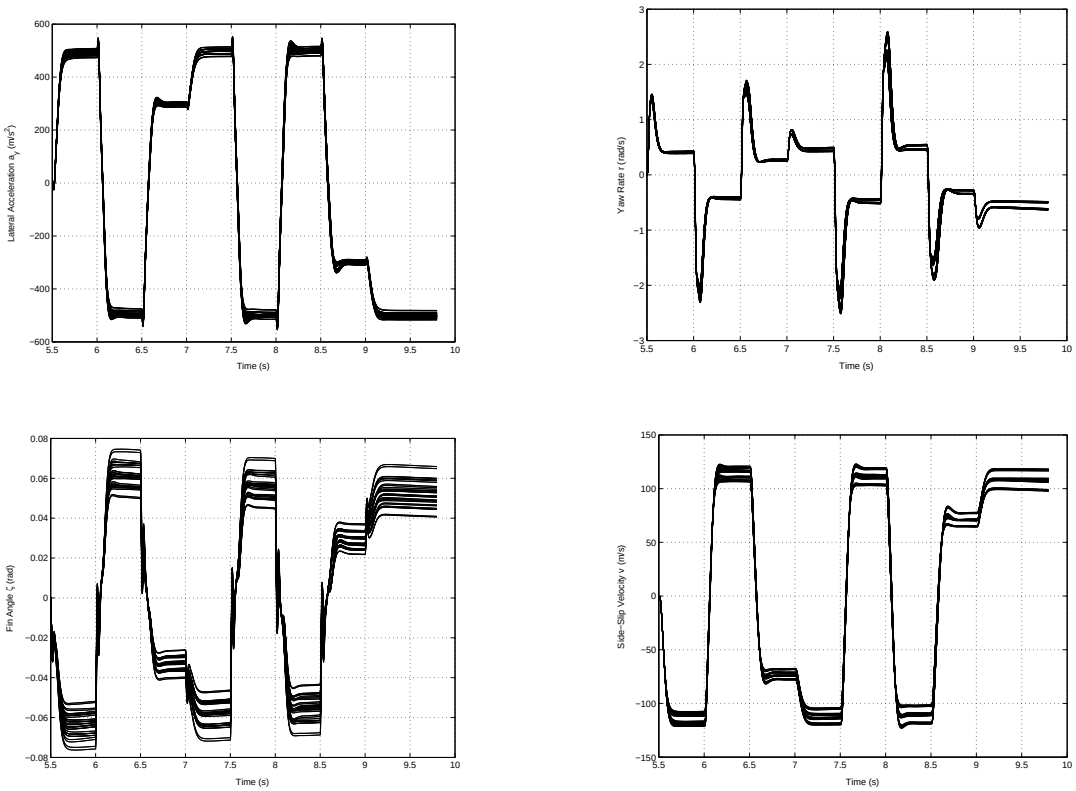

Figure 17: Lateral Acceleration Control Responses.

indeed a robust tracking controller for all possible perturbations.

Bibliography

[Chen et al., 1998] Chen, W.-H., Ballance, D. J., and Li, Y. (1998). Automatic loop-shaping in qft using genetic algorithms. Technical report, Centre for Systems and Control, University of Glasgow, Glasglow, UK.

[Deb, 2001] Deb, K. (2001). *Multi-Objective Optimization using Evolutionary Algorithms*. Wiley-Interscience Series in Systems and Optimization. John Wiley and Sons, Chichester.

[Franklin et al., 1994] Franklin, G. F., Powell, J. D., and Emami-Naeini, A. (1994). *Feedback Control of Dynamic Systems*. Addison-Wesley, Reading, Massachusetts, third edition.

[Horton, 1992] Horton, M. P. (1992). A study of autopilots for the adaptive control of tactical guided missiles. Master's thesis, University of Bath, Bath, UK.

[Houpis and Rasmussen, 1999] Houpis, C. H. and Rasmussen, S. J. (1999). *Quantitative Feedback Theory: Fundamentals and Applications*. Control Engineering. Marcel Dekker, New York.

[Hughes et al., 2003] Hughes, E. J., Tsourdos, A., and White, B. A. (2003). Multi-objective fuzzy design of a lateral autopilot for a quasi-linear parameter varying missile. In *Preprint of the IFAC Conference on Intelligent Control Systems and Signal Processing*, volume 1, pages 239–244, Algrave.

[Sidi, 2001] Sidi, M. (2001). *Design of Robust Control Systems: From Classical to Modern Practical Approaches*. Krieger, Malabar, Florida.

[Stilwell and Rugh, 2000] Stilwell, D. J. and Rugh, W. J. (2000). Stability preserving interpolation methods for the synthesis of gain scheduled controllers. *Automatica*, 36:665–671.